


Equine lung decellularization: a potential approach for in vitro modeling the role of the extracellular matrix in asthma

Journal of Tissue Engineering
Volume 9: 1–11
© The Author(s) 2018
Article reuse guidelines:
sagepub.com/journals-permissions
DOI: 10.1177/2041731418810164
journals.sagepub.com/home/tej



Renata Kelly da Palma^{1,2} , Paula Fratini²,
Gustavo Sá Schiavo Matias², Andressa Daronco Cereta²,
Letícia Lopes Guimarães², Adriana Raquel de Almeida Anuniação²,
Luis Vicente Franco de Oliveira³, Ramon Farre^{4,5,6}
and Maria Angelica Miglino²

Abstract

Contrary to conventional research animals, horses naturally develop asthma, a disease in which the extracellular matrix of the lung plays a significant role. Hence, the horse lung extracellular matrix appears to be an ideal candidate model for in vitro studying the mechanisms and potential treatments for asthma. However, so far, such model to study cell–extracellular matrix interactions in asthma has not been developed. The aim of this study was to establish a protocol for equine lung decellularization that maintains the architecture of the extracellular matrix and could be used in the future as an in vitro model for therapeutic treatment in asthma. For this the equine lungs were decellularized by sodium dodecyl sulfate detergent perfusion at constant gravitational pressure of 30 cmH₂O. Lung scaffolds were assessed by immunohistochemistry (collagen I, III, IV, laminin, and fibronectin), scanning electron microscopy, and DNA quantification. Their mechanical property was assessed by measuring lung compliance using the super-syringe technique. The optimized protocol of lung equine decellularization was effective to remove cells (19.8 ng/mg) and to preserve collagen I, III, IV, laminin, and fibronectin. Moreover, scanning electron microscopy analysis demonstrated maintained microscopic lung structures. The decellularized lungs presented lower compliance compared to native lung. In conclusion we described a reproducible decellularization protocol that can produce an acellular equine lung feasible for the future development of novel treatment strategies in asthma.

Keywords

Equine lung, decellularized, extracellular matrix, asthma, respiratory diseases

Date received: 21 May 2018; accepted: 10 October 2018

Introduction

According to World Health Organization,¹ 235 million people currently suffer from asthma and 383,000 deaths are attributed to this disease each year. The prevalence of

asthma is continuing to grow, and the overall prevalence is estimated to increase up to 100 million at 2025.¹ In this context, intensive scientific efforts to understand the disease and to find new treatments are required. However,

¹Post Graduate Program in Science of Rehabilitation, University Nove de Julho (UNINOVE), São Paulo, Brazil

²Department of Surgery, School of Veterinary Medicine and Animal Science, University of São Paulo, São Paulo, Brazil

³Medical School, University Center of Anápolis—UniEVANGÉLICA, Anápolis, Brazil

⁴Unitat Biofísica i Bioenginyeria, Facultat de Medicina i Ciències de la Salut, Universitat de Barcelona, Barcelona, Spain

⁵CIBER de Enfermedades Respiratorias, Madrid, Spain

⁶Institut d'Investigacions Biomèdiques August Pi i Sunyer, Barcelona, Spain

Corresponding author:

Maria Angelica Miglino, Department of Surgery, School of Veterinary Medicine and Animal Science, University of São Paulo, São Paulo, 05508-270, Brazil.

Email: miglino@usp.br



Creative Commons Non Commercial CC BY-NC: This article is distributed under the terms of the Creative Commons

Attribution-NonCommercial 4.0 License (<http://www.creativecommons.org/licenses/by-nc/4.0/>) which permits non-commercial use, reproduction and distribution of the work without further permission provided the original work is attributed as specified on the SAGE and Open Access page (<https://us.sagepub.com/en-us/nam/open-access-at-sage>).

Table 1. Merits and demerits between asthma models (pig, guinea pig, horse, and mouse).

Species	Disease models	Merits	Demerits
Pig	Induced by ovalbumina and spontaneous disease	<ul style="list-style-type: none"> Anatomy, biochemistry, physiology, size, and genetics of pigs resemble those of humans 	<ul style="list-style-type: none"> To establish chronic asthma model is difficult because the sensitivity to the antigen declines after repeated allergen exposure
Guinea pig	Induced by ovalbumina, ozone, viral infections, and spontaneous disease	<ul style="list-style-type: none"> Good for lung function studies; Neuroendocrine cells and neuroepithelial bodies are also localized to the epithelium like in humans; Airway smooth muscle closely resembles human airway smooth muscle. 	<ul style="list-style-type: none"> Spontaneous respiratory inflammation has not been fully explored; Due to the size of the airways and the limited number of cells recoverable, few studies of muscle proliferation and/or muscle synthesizing activity have been completed; Axon reflex is improbable to be present in human airways.
Mouse	Induced by ovalbumina, house dust mite, cockroach, and fungal extracts	<ul style="list-style-type: none"> Have contributed to our understanding of the T1/T2 disease paradigm 	<ul style="list-style-type: none"> Mouse and human eosinophils differ significantly from one another at molecular level; Differences in lung size, structure, and physiologic responses; Several compounds effective in rodent models of allergic airways disease were found to be ineffective as therapy for both RAO and human asthma.
Horse	Spontaneous disease	<ul style="list-style-type: none"> Parallel mechanisms of human asthma disease; RAO includes airway inflammation with neutrophil predominance, while IAD, is a related disorder with a mixed neutrophil/eosinophil phenotype; Ability to perform serial bronchoscopies, tissue biopsies, and determination of lung volumes by spirometry, both measurements are impractical in rodents; The equine genome has been sequenced, and an equine tissue bank has been developed for lung research. 	<ul style="list-style-type: none"> Asthma with fixed airflow limitation and obesity has insufficient evidence in horse

RAO: recurrent airway obstruction; IAD: inflammatory airway disease.

it is important to note that some therapeutic strategies for asthma previously derived from animal models in mice and rats have been failed when translated to human.²⁻⁴ A reason explaining this deceiving result is differential different transcriptional responses to acute inflammatory in rodents and humans.⁵ Interestingly, horses naturally develop an asthma-like condition currently known as recurrent airway obstruction (RAO), severe equine asthma,⁶ and inflammatory airway disease (IAD), a mild-to-moderate asthma.⁷ Therefore, asthma in the horse seems to be an unique animal model for better understanding the pathways implicated in this disease⁸ as demonstrated in Table 1.

Asthma is characterized by chronic airway inflammation which induces an abnormal extracellular matrix (ECM) deposition resulting in irreversible structural lung damage.^{9,10} Unfortunately, the specific anti-remodeling treatments of

asthma are still a scientific challenge¹⁰ requiring a better understanding of ECM remodeling for future treatments. It is remarkable that prolonged use of corticosteroids or combination therapy in asthma interferes on ECM elements.¹¹ It is remarkable that the ECM is an ideal candidate model for establishing an in vitro setting for research due to three-dimensional architecture, the biochemical composition, and the important role in the regulation of cell function and tissue regeneration.¹²

In recent years, lung bioengineering had been emerged as a potential future therapeutic alternative for treatment of respiratory diseases.¹³⁻¹⁶ The current approach to lung bioengineering is based on using the decellularized organ matrix. In addition to being used for applications such as repair and reconstruction,^{13,17} the decellularized lung matrix has been a useful tool to study cell-matrix interactions in lung disease.¹⁸ Furthermore, decellularized organ

scaffolds are used as *in vitro* ECM model reproducing the *in vivo* cell microenvironment thereby becoming a powerful model for studying the comprehensive roles of ECM in lung diseases¹⁹ and new approach for finding therapeutic solutions. However, obtaining a suitable lung decellularized matrix for studying mechanisms such as repair or cell–matrix interactions, it is required to preserve the native airway and vascular structure and retain key ECM components, which requires a fine-tuned decellularization protocol. Therefore, the aim of this study was to establish a protocol for equine lung decellularization for obtaining well-preserved ECM architecture for being used as a novel *in vitro* model for better understanding and treating asthma.

Methods

The experimental procedures were approved by the Ethical Committee for Animal Research of the University of São Paulo and carried out in accordance with the National Institutes of Health guide for the care and use of laboratory animals (NIH Publications no. 8023, revised 1978).

Animals

Animal tissue specimens were collected from the lungs of six healthy horses that had been slaughtered at the Veterinary Hospital from the University of São Paulo. All horses from which lungs were obtained had been declared as healthy by the state veterinarian or an inspector under the supervision of the veterinarian within 24 h prior to death. Lungs were excised within 30 min after sacrifice and stored at -80°C until the decellularization process was carried out.

Lung decellularization

Prior to starting the decellularization process, the accessory lobe of each lung was selected and placed into the experimental system with at a constant pressure of 30 cmH_2O (Figure 1). The lung lobe were washed three times via the airways and three times via the vasculature by instilling 5 L of phosphate-buffered saline (PBS) 1 \times containing streptomycin (90 mg/mL), penicillin (50 U/mL), and amphotericin B (25 mg/mL) until the liquid extracted from the lungs had a transparent appearance. This step was repeated with 2 L de-ionized water and subsequently treated with instillation of 4 L 1% sodium dodecyl sulfate (SDS) detergent. The lung lobes were subsequently kept in agitation for 24 h at room temperature in a 4-L plastic bucket, with 1 L of 1% SDS; and this process was repeated for 3 days. At day 5, the lung lobes were rinsed again with 5 L PBS 1 \times (with the antibiotic/antimycotic components described above) and maintained in 1 L PBS 1 \times in agitation for 24 h to finish the process for obtaining acellular lung scaffolds. All the rinses were instilled until the lung lobe was fully inflated. At this

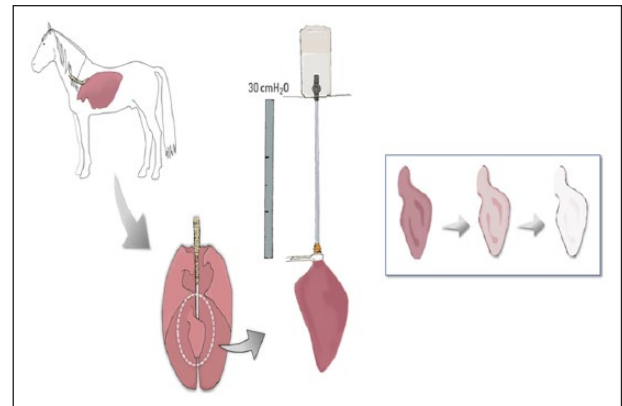


Figure 1. Schematic illustration of the system for equine lung decellularization.

point, we stopped the instillation and the lobes were allowed to passively drain and are also manually manipulated to assist the removal of the liquid before proceeding with the next filling to avoid high-pressure-induced damage.

Decellularization assessment

Three native and three decellularized lungs were fixed by submersion in 4% paraformaldehyde for at least 3 h at room temperature, embedded in paraffin, sliced into 5 μm sections, and mounted on glass slides. Following deparaffinization, sections were stained with hematoxylin and eosin (H&E) in order to verify the absence of cellular DNA and with colloidal iron for assessing ECM structure (collagen, glycosaminoglycans, and cytoplasm) after the decellularization process. The images were captured using Nikon Eclipse 80I microscope, ensuring that the various areas of the sample are cell-free after decellularization.

In addition, the level of remaining DNA in the scaffold after the decellularization procedure was measured in three randomly selected decellularized lungs and in two native lungs. A sample of small piece from the accessory lobe was dried and weighted, and its total genomic DNA was isolated using the spin-column-based PureLink[®] Genomic DNA Mini Kit (Invitrogen[™]) according to manufacturer's instructions. Double-stranded DNA yield was measured using spectrophotometry (NanoDrop 1000; Thermo Scientific) and normalized to sample tissue weight.

To perform immunohistochemistry imaging, paraffin-embedded samples of the lung (5-mm thick) obtained from each group were sectioned in microtome (#RM2265; Leica) and transferred to poly-L-lysine (#p8920; Sigma) treated glass slides. The sections were rehydrated and microwaved in citrate buffer (1.83 mM of monohydrate citric acid and 8.9 mM of sodium citrate tribasic dehydrate; pH 6.0) for antigen retrieval. The endogenous peroxidase block was performed with 3% hydrogen peroxide in distilled water for 30 min in the dark. Nonspecific protein interaction was

blocked with 2% of bovine serum albumin (BSA) in PBS for 30 min. Primary antibodies such as anti-collagen I (#600-401-103 S, 1:400; Rockland), anti-collagen III (#sc-8779, 1:100; Santa Cruz), anti-collagen IV (#1-CO083-0, 1:500; Quartett), anti-laminin subunit alpha-2 (#bs-8561R, 1:200; Bioss Antibodies), and anti-fibronectin (#NBP1-91258, 1:200; Novus Biologicals) were incubated overnight in humid chamber at 4°. The reaction was detected by Dako Advance HRP (#K6068; Dako) and the color developed with DAB (#K3468; Dako) according to the manufacturer's instructions. The slides were lightly counter-stained with hematoxylin. Between each step, after antibody incubation, the slides were rinsed in PBS containing 0.2% of BSA. Finally, slides were mounted and visualized at Nikon Eclipse 80I microscope.

For quantifying collagen area, the tissue samples were fixed with 10% buffered formalin, embedded in paraffin, and stained with picrosirius red. The stained sections were imaged at high ($\times 200$) magnification with a Nikon Eclipse 80I microscope. A total of 12 fields from each stained section were analyzed using ZEN Blue 2.3 software (Carl Zeiss). As shown in Figure 6, the collagen was stained with red and the collagen area was obtained from a combination of SD from mean signal and isodata automatic thresholding.

Scanning electron microscopy

Slices of the decellularized lungs and control were prepared for imaging. The samples for scanning electron microscopy (SEM) were fixed with 2% glutaraldehyde and 2.5% paraformaldehyde in 0.1-M cacodylate buffer (EMD Biosciences) for 2 h at room temperature, rinsed in cacodylate buffer, and dehydrated through an ethanol gradient. The samples were further dehydrated in hexamethyldisilazane for 10 min and dried overnight, sputter-coated with gold, and analyzed using the scanning electron microscope Hitachi Analytical Table Top Microscope TM3000 (Hitachi) with 15-kVa acceleration.

Measurement of lung compliance

Compliance was assessed as the volume–pressure ratio from values obtained using the super-syringe technique.²⁰ This method consists of inflating of the lung lobe in steps of 100 mL with a syringe until a volume of 1000 mL. Airway inflation pressure was measured with a water column in cmH_2O with reference to atmospheric pressure.

Acellular lung matrix scaffold recellularization

To confirm whether decellularized horse lung can be recellularized and to verify the adhesion molecules, we used two different cell types. Horse dermal fibroblasts were harvested, cultured, and characterized as previously described.²¹ An amount of 5×10^4 fibroblasts were plated on untreated

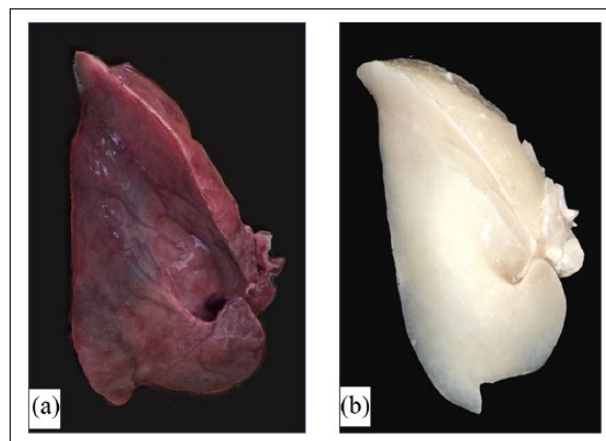


Figure 2. Representative example of (a) an intact and (b) a decellularized equine lung.

plates (Sarstedt) containing slices of horse lung scaffolds for 5 days. In addition, canine yolk sac cells transduced with vascular endothelial growth factor–enhanced green fluorescent protein (VEGF_eGFP; yolk sac VEGF (YSVEGF)) previously characterized by our group²² were seeded (5×10^4 cells) on untreated plates (Sarstedt) containing slices of horse lung scaffolds for 5 days.

Immunocytochemistry

The plates containing the fibroblast or YS/YSVEGF cells and scaffolds were fixed with 4% paraformaldehyde. The scaffolds were washed with PBS + 0.5% Tween and incubated with the primary antibody fibronectin (Abcam) at 1:200 dilution. Then, the fibroblast and YS/YSVEGF cells were washed in PBS + 0.5% Tween and the secondary antibody Alexa Fluor 594 (Thermo Fisher). To investigate cell adhesion on scaffold, the following biomarkers were used: N-cadherin and CD31. Plates were incubated with 4',6-diamidino-2-phenylindole (DAPI) for nuclear labeling. Samples were analyzed on Confocal Microscope—Olympus Fluoview 1000 (FV1000).

Statistical analysis

The values are expressed as mean \pm standard error (SE). Values of lung compliance, DNA quantification, and collagen area (%) between native and decellularized lung values were evaluated by means of paired t-tests. Statistical significance was considered when $p < 0.05$.

Results

As expected from previous studies from mice lung,²³ our protocol based on constant-pressure decellularization media perfusion did not result in alterations in terms of maintenance of scaffold structure and composition of main ECM component after lung decellularization (Figure 2).

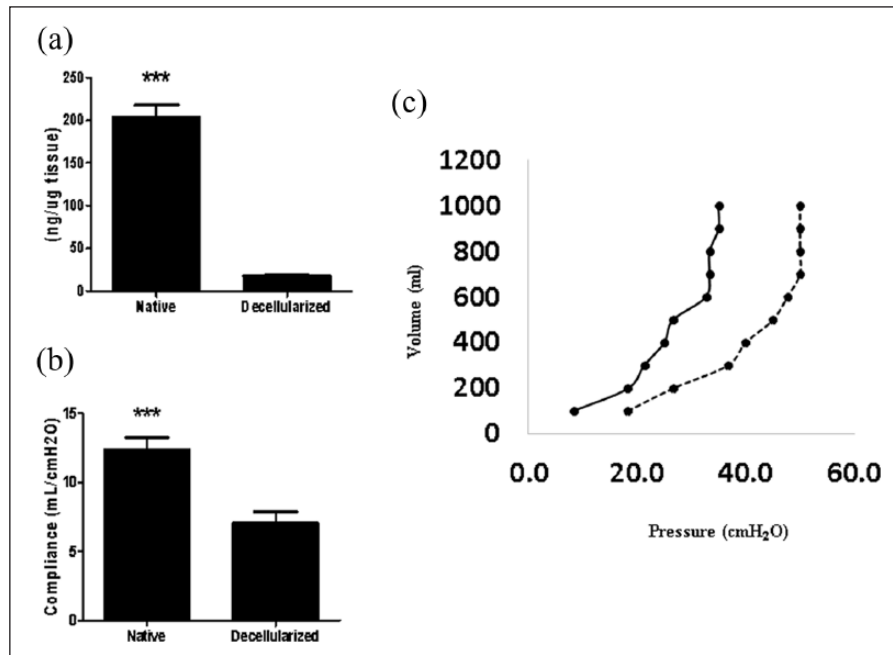


Figure 3. (a) DNA quantification before and after equine lung decellularization. (b) Lung compliance before and after decellularization. (c) Pressure/volume (P/V) values assessed using the super-syringe technique with inflation of the lungs in steps of 100 mL up to 1 L. Native lung is represented as [—] and decellularized lung as [---]. Data are represented as mean \pm SE.

Lung scaffolds obtained by decellularization showed genomic DNA content in the 17.75 ± 2.05 ng/mg (below the 50 ng/mg suggested by Crapo et al.²⁴) (Figure 3(a)) and lacked cellular nuclei assessed by H&E (Figure 4).

As shown in Figure 5, the collagen area was lower in decellularized lungs (3.70 ± 0.46) as compared with native lungs (13.43 ± 1.67), and the components of the ECM such as glycosaminoglycans (Figure 4), elastin, fibronectin, and collagen I, III, and IV remained similar in both groups (Figure 6). Furthermore, observation by SEM showed that the microscopic lung structures were also well maintained (Figure 5).

Pressure–volume measured (Figure 3(b)) showed that decellularized lungs were stiffer than native lungs, as indicated by decreased compliance (native: 12.32 ± 0.92 vs decellularized: 7.04 ± 0.81 mL/cmH₂O) and P/V values (Figure 3(c)).

The immunocytochemical analysis confirmed the presence of YSVEGF and fibroblast cells in the acellular equine lung matrix (Figures 7, 8, 9 and 10).

Discussion

We believe that this work will be relevant for future studies in the field of lung diseases. Considering that lung diseases in horses such as asthma present similarities to human, it becomes an ideal model for studying mechanism and treatment in asthma using the decellularized ECM as an *in vivo* model. The decellularized lung can be used for repair, reconstruction, and to study cell–matrix interactions in lung disease.^{13,18} Therefore, we demonstrated in this study

that our protocol created an optimal lung scaffold with the necessary balance between removal of the native cell population and maintaining the pulmonary structures.

Acellular lung scaffold from large animal seems to be ideal for translation into clinical studies in humans^{25,26} when compared to rodent models.⁵ Experimental large animals more used for lung decellularization protocol are porcine²⁷ and non-human primate,^{25,26} which these models offer the advantage of closely resembling the biology of humans.²⁶ By contrast, this is the first study to date using equine lung for creating an organ scaffold. This large animal model presents similarities with human neutrophilic asthma²⁸ including the remodeling of ECM and similar biology.²⁹ Considering that many experiments are not possible in humans because of ethical considerations, use of this model can be a milestone in the field of respiratory diseases.

Several techniques of lung decellularization have been developed in the last years, which retain ECM proteins and three-dimensional architecture.^{13–16,23} The approach frequently utilized is detergent-based decellularization including SDS, Triton X100, sodium deoxycholate (SDC), and 3-((3-cholamidopropyl)dimethylammonio)-1-propanesulfonate (CHAPS). In this work, we based our lung decellularization process in previous studies using SDS 1%,^{23,30–32} which is a cheap detergent and more efficient for removing cell residue tissue and increased ECM retention when compared to other detergents.^{33,34} Given that it resulted in a residual DNA level less than 50 ng of DNA per 1 mg of dry weight of the ECM scaffold (19.8 ng/mg), the protocol employed for equine lung decellularization seems suitable.²⁴

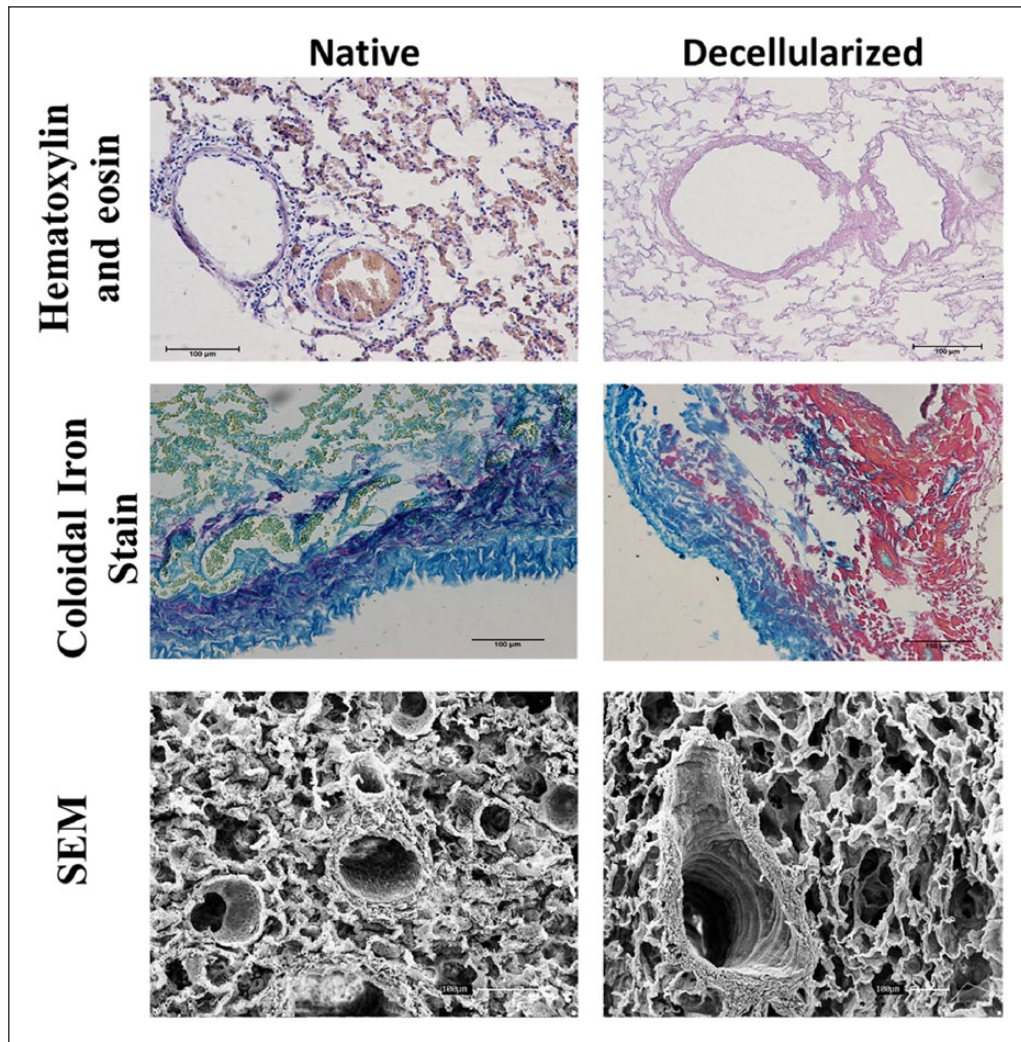


Figure 4. Representative native and decellularized equine lung tissue, as visualized by hematoxylin and eosin (H&E), colloidal iron stain, and SEM images. Sections indicate maintenance of tissue architecture, ECM, removal of debris and blood, and lack of visible nuclear material.

Other criteria defining adequate decellularization of scaffolds address retention of specific ECM components (collagen I, III, IV, laminin, fibronectin, and glycosaminoglycans) and maintenance of structures.³⁵ Collagen I is a major component of the ECM and along with collagen IV is a critical component of fibrillar basement membrane for lung transplantation after decellularization.³⁶ Collagen III is the second most abundant collagen type and provides the structure of the pulmonary blood vessels, alveolar wall, visceral pleura, and the connective tissue around the tracheobronchial tree,³⁷ structures to be preserved for future recellularization. Laminin plays a key role in epithelial cell matrix motility and adhesion after recellularization;³⁸ glycosaminoglycans is determinant of mechanical behavior of lung tissue, while fibronectin plays a role in cell adhesion, growth, migration, and differentiation.³⁵ Although Petersen et al.³⁹ demonstrated that SDS induced a greater loss of

type-1 collagen and elastin when compared to CHAPS, Gilpin et al.²⁷ showed greatest preservation of ECM components in SDS-decellularized lungs in comparison with CHAPS and SDC. We believe that concentration of SDS can have an influence on three-dimensional maintenance, collagen, and elastin.⁴⁰ Perfusing 1% SDS solution preserved all these ECM proteins in the lung scaffold obtained from this study thereby corroborating other published studies.^{23,31,41–43}

Although our work demonstrates that the ECM retains some important proteins after decellularization process, we found differences in relation to mechanical pulmonary properties. Some previous studies have measured the P/V curves in decellularized lungs in mice,¹⁵ pig,⁴ and human^{16,44} models, with no previous data available for equine lungs. Interestingly and in agreement with Price et al.,^{15,16} our results indicate that decellularized horse

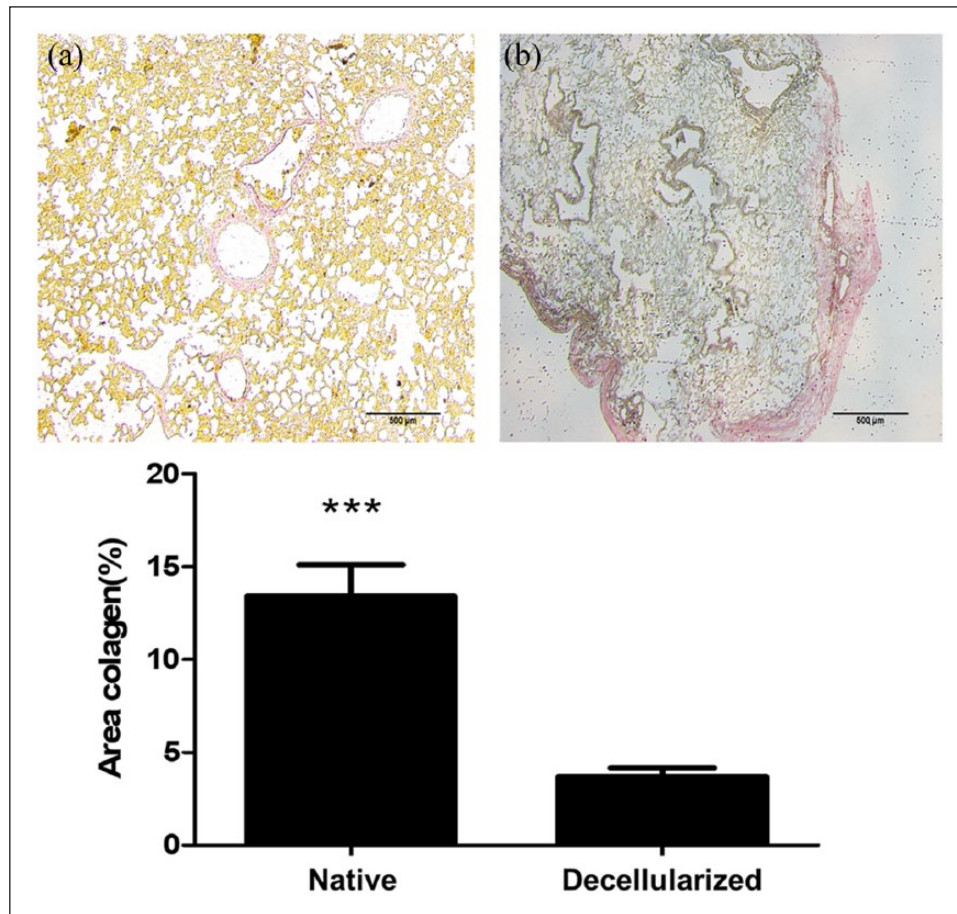


Figure 5. Representative histological analysis for collagen quantification of (a) native and (b) decellularized equine lung tissue. The lung tissue samples were stained with picosirius red (red = collagen). Bar graph shows collagen area (%). Asterisk indicates significance of difference between the groups (* $p < 0.005$; ** $p < 0.05$).

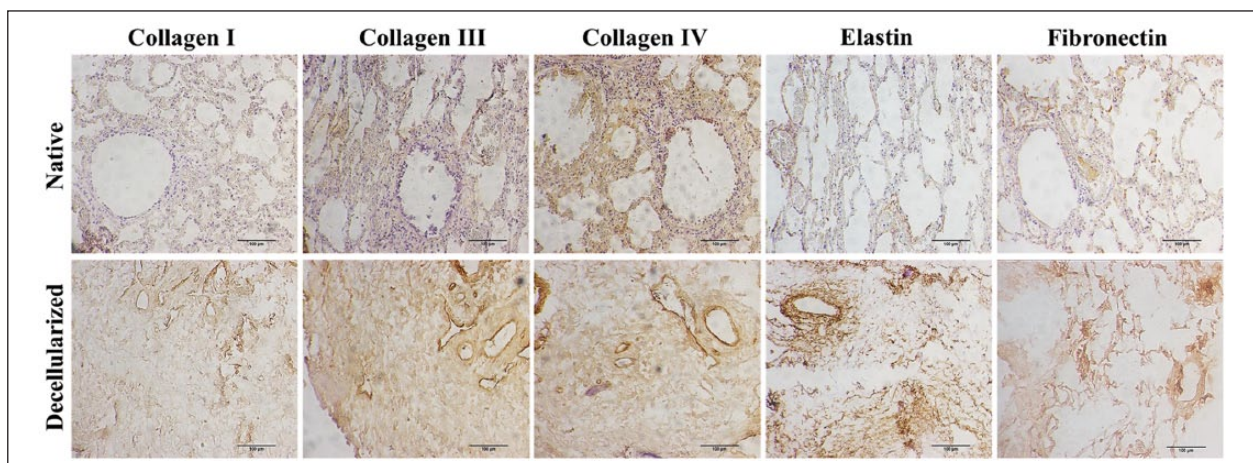


Figure 6. Immunohistochemistry images of native and decellularized equine lung slices stained for different components of the extracellular matrix (collagen I, III, IV, fibronectin, and elastin). Scale bar = 100 μm .

lungs were less compliant, that is, more stiff than native lungs probably due to loss of surfactant and cells after decellularization.^{15,16,45}

A limitation of this study was that we did not compare our decellularization equine lung protocol with cells from other species. However, it should be noted that in this

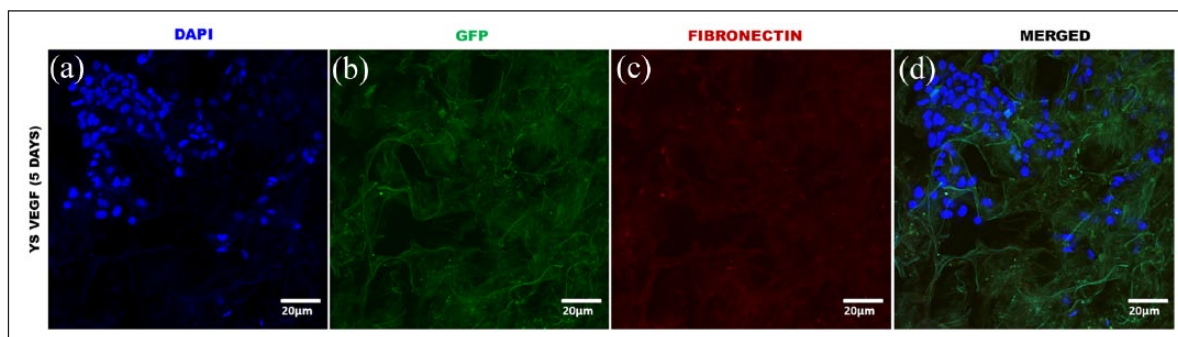


Figure 7. Immunocytochemistry of equine lung scaffolds with YSVEGF. (a) DAPI nuclei YSVEGF cells in scaffold of equine lung; (b) marked presence of YSVEGF cells expressing eGFP; (c) scaffold of lung expressing fibronectin in red; (d) presence of these cells in the scaffold in red that expresses fibronectin is very clear, proving the efficient recellularization.

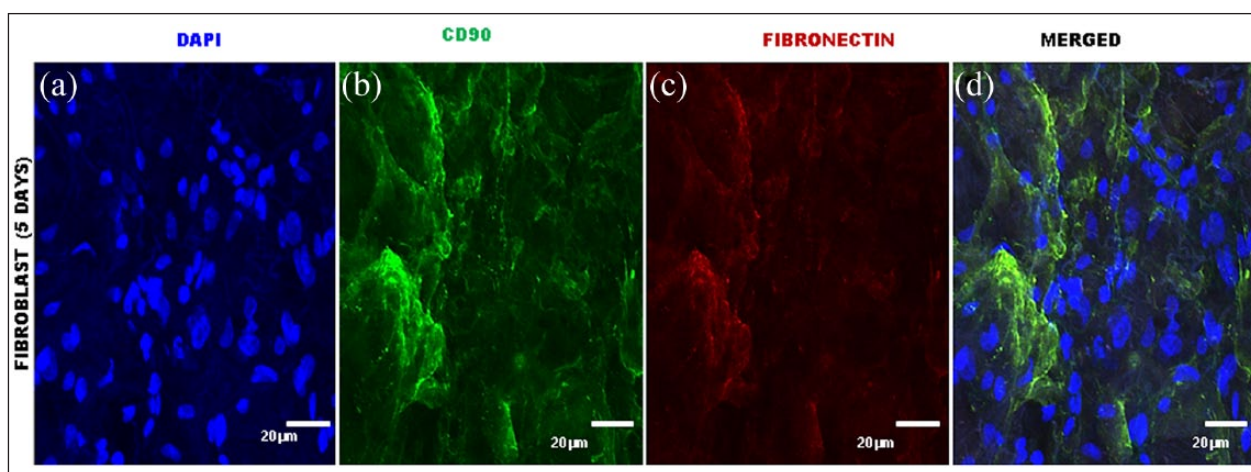


Figure 8. Immunocytochemistry of equine lung scaffolds with fibroblast cells. (a) DAPI nuclei of fibroblast cells; (b) marked presence of fibroblast cells expressing CD90 in green; (c) marked presence in lung scaffold of expressing fibronectin in red; (d) presence of these cells in the scaffold that expresses fibronectin is very clear, proving the efficient recellularization.

study, to test the viability of recellularization in equine acellular lung, we use cells obtained from different species (equine and cat) and types (fibroblast and endothelial). Although our protocol showed a decrease in total collagen, we produced a suitable scaffold for cell growth and adherence, similar to results obtained by Sengyoku et al.⁴⁶ Therefore, further studies are necessary to better investigate cell seeding and culturing on the equine decellularized lung.

The approaches commonly utilized for lung decellularization include perfusion of reagents through lung vasculature and/or airways. Previous studies demonstrated that the perfused SDS detergent through the pulmonary artery^{23,32,43} or airways^{30,31,47} resulted in a suitable acellular lung with retention of specific ECM components and removal of cells. In this study, we infused decellularization agents through both combined routes, vascular and airway, by applying a constant physiological pressure of 30 cmH₂O. According to previous studies, monitoring constant pressure can avoid damage triggered by manual pressure since

variability between investigators and experiments is reduced.^{16,32,43,44} Specifically, this protocol by constant pressure infusion of decellularizing agents is able to retain critical ECM proteins and to maintain lung scaffold structure and microvasculature as indicated by SEM analyses and immunohistochemistry (Figures 4 and 6).

Conclusion

In conclusion, we described a reproducible decellularization protocol that can produce an equine acellular lung which is a feasible tool for the future development of novel basic and translation research and drug-testing strategies in asthma. This study may be very relevant in the field of lung disease modeling considering the given unique similarities between humans and equine lungs in terms of asthma development. Actually, equine acellular lung scaffolds can be elaborated into commercial production lines to make available high-throughput tests in asthma pharmacology.

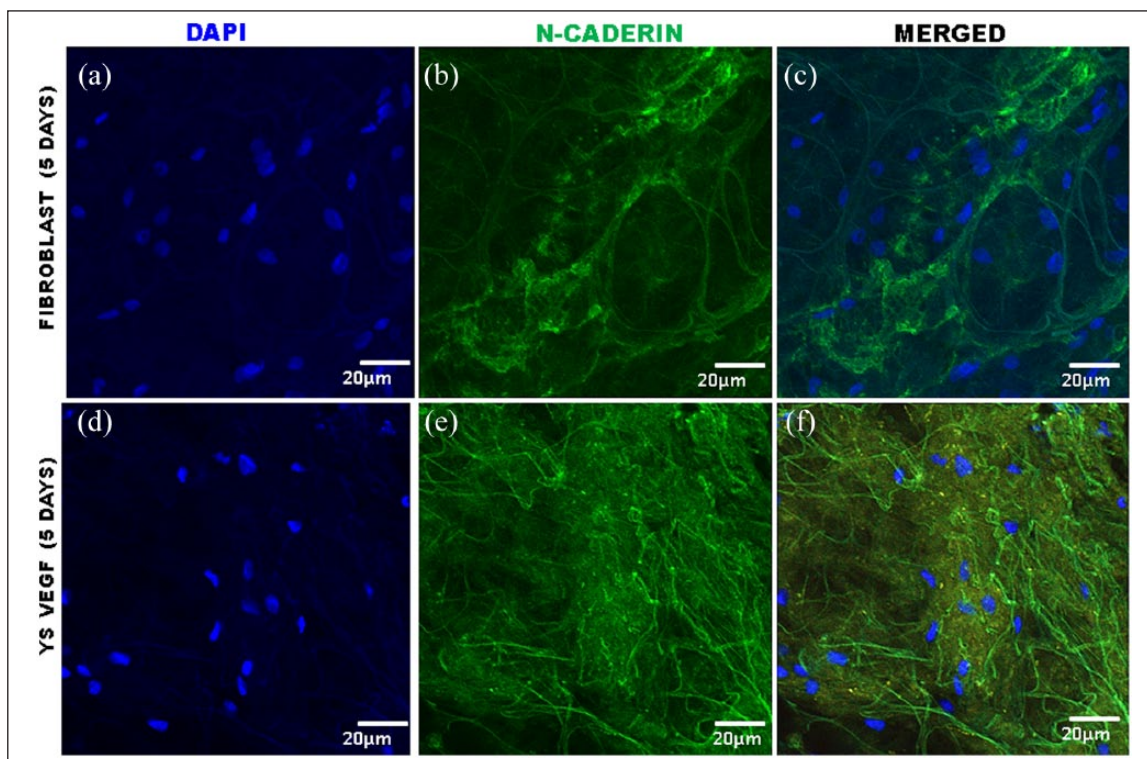


Figure 9. Immunofluorescence of equine lung scaffolds for expression of N-cadherin, a biomarker for adhesion cell. (a) DAPI nuclei of fibroblast cells; (b) expression of N-cadherin; (c) presence in equine lung scaffold of DAPI and N-cadherin; (d) DAPI nuclei of YSVEGF; and (e) expression of N-cadherin; (f) presence in equine lung scaffold of DAPI and N-cadherin.

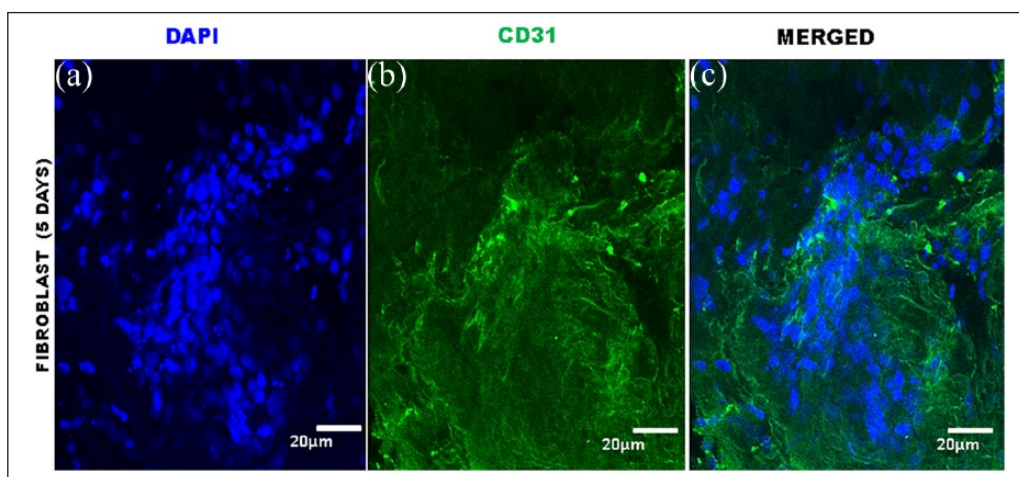


Figure 10. Immunofluorescence of equine lung scaffolds for expression of CD31, a biomarker for adhesion cell. (a) DAPI nuclei of fibroblast cells and (b) expression of CD31; (c) presence in equine lung scaffold of DAPI and CD31.

Declaration of conflicting interests


The author(s) declared no potential conflicts of interest with respect to the research, authorship, and/or publication of this article.

Funding

The author(s) disclosed receipt of the following financial support for the research, authorship and/or publication of this article:

This work was supported by the Fundação de Amparo e Pesquisa de São Paulo (grant no. 2014/50844). The authors are thankful to the Advanced Center of Image Diagnosis (CADI-FMVZ-USP) facility and staff for technical support.

ORCID iD

Renata Kelly Palma  <https://orcid.org/0000-0002-4799-0385>

References

- World Health Organization. Media centre fact sheets as of April 2017, <http://www.who.int> (accessed 3 September 2017).
- Clienti S, Morjaria JB, Basile E, et al. Monoclonal antibodies for the treatment of severe asthma. *Curr Allergy Asthma Rep* 2011; 11: 253–260.
- Giembycz MA and Newton R. Harnessing the clinical efficacy of phosphodiesterase 4 inhibitors in inflammatory lung diseases: dual-selective phosphodiesterase inhibitors and novel combination therapies. *Handb Exp Pharmacol* 2011; 204: 415–446.
- Nair P, Gaga M, Zervas E, et al. Safety and efficacy of a CXCR2 antagonist in patients with severe asthma and sputum neutrophils: a randomized, placebo-controlled clinical trial. *Clin Exp Allergy* 2012; 42: 1097–1103.
- Seok J, Warren HS, Cuenca AG, et al. Genomic responses in mouse models poorly mimic human inflammatory diseases. *Proc Natl Acad Sci U S A* 2013; 9: 3507–3512.
- Robinson NE. International workshop on equine chronic airway disease. Michigan State University 16–18 June 2000. *Equine Vet J* 2001; 33: 5–19.
- Couetil LL, Hoffman AM, Hodgson J, et al. Inflammatory airway disease of horses. *J Vet Intern Med* 2007; 21: 356–361.
- Bullone M and Lavoie JP. Asthma “of horses and men”—how can equine heaves help us better understand human asthma immunopathology and its functional consequences? *Mol Immunol* 2015; 66: 97–105.
- Benayoun L, Druilhe A, Dombret MC, et al. Airway structural alterations selectively associated with severe asthma. *Am J Respir Crit Care Med* 2003; 167: 1360–1368.
- Bullone M, Vargas A, Elce Y, et al. Fluticasone/salmeterol reduces remodelling and neutrophilic inflammation in severe equine asthma. *Sci Rep* 2017; 7: 8843.
- Burgess JK, Mauad T, Tjin G, et al. The extracellular matrix—the under-recognized element in lung disease? *J Pathol* 2016; 4: 397–409.
- Hoshihara T, Chen G, Endo C, et al. Decellularized extracellular matrix as an in vitro model to study the comprehensive roles of the ECM in stem cell differentiation. *Stem Cells Int* 2016; 2016: 6397820.
- Ott HC, Clippinger B, Conrad C, et al. Regeneration and orthotopic transplantation of a bioartificial lung. *Nat Med* 2010; 16: 927–933.
- Song JJ, Kim SS, Liu Z, et al. Enhanced in vivo function of bioartificial lungs in rats. *Ann Thorac Surg* 2011; 92: 998–1005.
- Price AP, England KA, Matson AM, et al. Development of a decellularized lung bioreactor system for bioengineering the lung: the matrix reloaded. *Tissue Eng Part A* 2010; 16: 2581–2591.
- Price AP, Godin LM, Domek A, et al. Automated decellularization of intact, human-sized lungs for tissue engineering. *Tissue Eng Part C Methods* 2015; 21: 94–103.
- Petersen TH, Calle EA, Zhao L, et al. Tissue-engineered lungs for in vivo implantation. *Science* 2010; 329: 538–541.
- Sun H, Zhu Y, Pan H, et al. Netrin-1 regulates fibrocyte accumulation in the decellularized fibrotic sclerodermatous lung microenvironment and in bleomycin-induced pulmonary fibrosis. *Arthritis Rheumatol* 2016; 5: 1251–1261.
- Hoshihara T, Lu H, Kawazoe N, et al. Decellularized matrices for tissue engineering. *Expert Opin Biol Ther* 2010; 10(12): 1717–1728.
- Matamis D, Lemaire F, Harf A, et al. Total respiratory pressure-volume curves in the adult respiratory distress syndrome. *Chest* 1984; 86(1): 58–66.
- Li LF, Guan WJ, Hua Y, et al. Establishment and characterization of a fibroblast cell line from the Mongolian horse. *Vitro Cell Dev Biol Anim* 2009; 45(7): 311–316.
- Fratini P, Carreira AC, Alcântara D, et al. Endothelial differentiation of canine yolk sac cells transduced with VEGF. *Res Vet Sci* 2016; 104: 71–76.
- Da Palma RK, Campillo N, Uriarte JJ, et al. Pressure- and flow-controlled media perfusion differently modify vascular mechanics in lung decellularization. *J Mech Behav Biomed Mater* 2015; 49: 69–79.
- Crapo PM, Gilbert TW and Badylak SF. An overview of tissue and whole organ decellularization processes. *Biomaterials* 2011; 32(12): 3233–3243.
- Bonvillain RW, Danchuk S, Sullivan DE, et al. A nonhuman primate model of lung regeneration: detergent-mediated decellularization and initial in vitro recellularization with mesenchymal stem cells. *Tissue Eng Part A* 2012; 18(23–24): 2437–2452.
- Bonvillain RW, Scarritt ME, Pashos NC, et al. Nonhuman primate lung decellularization and recellularization using a specialized large-organ bioreactor. *J Vis Exp* 2013; 15(82): e50825.
- Gilpin SE, Ren X, Okamoto T, et al. Enhanced lung epithelial specification of human induced pluripotent stem cells on decellularized lung matrix. *Ann Thorac Surg* 2014; 98(5): 1721–1729; discussion 1729.
- Leclere M, Lavoie-Lamoureux A and Lavoie JP. Heaves, an asthma-like disease of horses. *Respirology* 2011; 16: 1027–1046.
- Bullone M, Moran K, Lavoie-Lamoureux A, et al. PI3K and MAPKs regulate neutrophil migration toward the airways in heaves. *J Vet Intern Med* 2013; 27: 164–170.
- Nonaka PN, Campillo N, Uriarte JJ, et al. Effects of freezing/thawing on the mechanical properties of decellularized lungs. *J Biomed Mater Res A* 2014; 102(2): 4139.
- Nonaka PN, Uriarte JJ, Campillo N, et al. Mechanical properties of mouse lungs along organ decellularization by sodium dodecyl sulfate. *Respir Physiol Neurobiol* 2014; 200: 1–5.
- Da Palma RK, Nonaka PN, Campillo N, et al. Behavior of vascular resistance undergoing various pressure insufflation and perfusion on decellularized lungs. *J Biomech* 2016; 49(7): 12302.
- Du L, Wu X, Pang K, et al. Histological evaluation and biomechanical characterisation of an acellular porcine cornea scaffold. *Br J Ophthalmol* 2011; 95: 410–414.
- Wallis JM, Borg ZD, Daly AB, et al. Comparative assessment of detergent-based protocols for mouse lung decellularization and re-cellularization. *Tissue Eng Part C Methods* 2012; 18: 420–432.
- Wagner DE, Bonvillain RW, Jensen T, et al. Can stem cells be used to generate new lungs? Ex vivo lung bioengineering

- with decellularized whole lung scaffolds. *Respirology* 2013; 18(6): 895–911.
36. Stabler CT, Lecht S, Mondrinos MJ, et al. Revascularization of decellularized lung scaffolds: principles and progress. *Am J Physiol Lung Cell Mol Physiol* 2015; 309: L1273–L1285.
 37. Dunsmore SE. Treatment of COPD: a matrix perspective. *Int J Chron Obstruct Pulmon Dis* 2008; 3: 113–122.
 38. Badylak SF, Taylor D, Uygun K, et al. Whole-organ tissue engineering: Decellularization and recellularization of three-dimensional matrix scaffolds. *Annu Rev Biomed Eng* 2011; 13: 27–53.
 39. Petersen TH, Calle EA, Colehour MB, et al. Matrix composition and mechanics of decellularized lung scaffolds. *Cells Tissues Organs* 2012; 195(3): 222–231.
 40. Tebyanian H, Karami A, Motavallian E, et al. Histologic analyses of different concentrations of TritonX-100 and Sodium dodecyl sulfate detergent in lung decellularization. *Cell Mol Biol* 2017; 63(7): 46–51.
 41. Gilpin SE, Charest JM, Ren X, et al. Regenerative potential of human airway stem cells in lung epithelial engineering. *Biomaterials* 2016; 108: 111–119.
 42. Guyette JP, Gilpin SE, Charest JM, et al. Perfusion decellularization of whole organs. *Nat Protoc* 2014; 9(6): 1451–1468.
 43. Melo E, Garreta E, Luque T, et al. Effects of the decellularization method on the local stiffness of acellular lungs. *Tissue Eng Part C Methods* 2014; 20(5): 412–422.
 44. Girard ED, Jensen TJ, Vadasz SD, et al. Automated procedure for biomimetic de-cellularized lung scaffold supporting alveolar epithelial transdifferentiation. *Biomaterials* 2013; 34(38): 10043–10055.
 45. Nichols JE, Niles J, Riddle M, et al. Production and assessment of decellularized pig and human lung scaffolds. *Tissue Eng Part A* 2013; 19(17–18): 2045–2062.
 46. Sengyoku H, Tsuchiya T, Obata T, et al. Sodium hydroxide based non-detergent decellularizing solution for rat lung. *Organogenesis* 2018; 14: 94–106.
 47. Uriarte JJ, Nonaka PN, Campillo N, et al. Mechanical properties of acellular mouse lungs after sterilization by gamma irradiation. *J Mech Behav Biomed Mater* 2014; 40: 168–177.